Adsorption (2023) 29:125–139
https://doi.org/10.1007/s10450-023-00382-2

Scale-up analysis of a twin-bed PSA pilot plant

A. Marcinek[1] · **P. Bárcia**[2] · **J. Guderian**[1]

Received: 25 July 2022 / Revised: 30 December 2022 / Accepted: 20 March 2023 / Published online: 10 April 2023

Abstract
Small-scale pressure swing adsorption (PSA) plants, also referred to as pilot plants, are commonly exploited for studying separation processes in favour of the development of mathematical models and scale-up strategies. The applicability of a lately presented mathematical model, which was developed based on experimental data acquired from a high-purity twin-bed N_2-PSA pilot plant, is verified in this paper for the design of large-scale systems by an analysis of the mass transfer zone development at different PSA cycle times. Effects of the PSA scale-up factor, adsorber aspect ratio, packed-bed density, and flow resistances along the piping system on the process performance are studied numerically. These considerations are particularly relevant for the scale-up of bank-type PSA units as well as for skid-mounted systems fitted to local space limitations, where the standard scale-up concept of keeping the gas velocity constant often cannot be fully realised. It is demonstrated that the sensitivity of the PSA performance to studied factors increases along with the required product purity level. Therefore, recommendations for adequate dimensions of pilot plants depending on the desired gas purity level can be derived. Limitations of the gas velocity through the adsorber shall be observed to generate reliable simulation data. The agreement between experimental results obtained from an industrial-scale system on one hand, and the outcome of a dynamic simulation on the other hand, is confirmed—provided that realistic pressure profiles are generated by a proper adjustment of flow resistances along the piping.

Keywords Pressure swing adsorption · Dynamic simulation · Plant scale-up · Aspen Adsorption

List of symbols

CMS	Carbon molecular sieve
Cv	Valve flow coefficient [kmol/s/bar]
d	Adsorbent pellet diameter [mm]
D	Packed-bed diameter [mm]
EXP	Experimental value
F	Flow rate [m^3_n/h]
HCT	Half-cycle time
L	Packed-bed length [mm]
MTZ	Mass transfer zone
SIM	Simulated value
U	Superficial velocity [m/s]
U_f	Minimum fluidisation velocity [m/s]
U_y	Superficial velocity of oxygen concentration front [m/s]
V	Packed-bed volume [L]
V_B	Adsorber bottom void volume [L]
V_R	Nitrogen receiver tank volume [L]
V_T	Adsorber top void volume [L]
y	Oxygen mole fraction in gas phase [kmol/kmol]
α	PSA scale-up factor [-]
ε_{bed}	Packed-bed porosity [-]
ρ_{app}	Adsorbent apparent density [kg/m^3]
ρ_{bed}	Packed-bed density [kg/m^3]
φ	Bed utilisation [%]
χ	Magnitude of the roll-up effect [kmol/kmol · mm

1 Introduction

Despite the fact that continuous processes for the separation and purification of gases by adsorption are well-established and commonly implemented in industrial practice, they are still subjected to incessant improvement. Especially pressure swing adsorption (PSA) and temperature swing adsorption

✉ A. Marcinek
marcinek.aleksandra@fh-muenster.de

[1] Department of Chemical Engineering, Muenster University of Applied Sciences, Stegerwaldstrasse 39, 48565 Steinfurt, Germany

[2] Technology and Engineering Department, Sysadvance©, Rua Comendador Brandão 461, 4495-375 Póvoa de Varzim, Portugal

(TSA) techniques for the advancement of CO_2 capture strategies are currently largely investigated [1–6]. Nevertheless, the development of cyclic adsorption systems in the fields of air separation, hydrogen recovery, or biogas upgrading is also ongoing [7–9]. Generally, three main points of focus shall be considered to enhance the performance of those methods; namely, (1) an upgrade of the adsorbents towards higher selectivity and/or adsorption capacity, (2) a modification of the cycle regime for a better adsorbent utilisation, and/or (3) a rearrangement of the plant construction for the optimisation of flow characteristics. The establishment of reliable, empirically verified performance intensification strategies becomes much more challenging and overpriced as the size of the plant approaches the industrial-scale. For that reason, small-scale PSA/TSA systems became an essential instrument among both suppliers and consumers of adsorbent materials. Typically, the volume of adsorber columns installed in pilot plants varies between 1 and 150 L. Yet, that relatively small adsorber volume allows a quick evaluation and verification of the adsorbent quality at small material quantity, as well as an investigation of suitable cycle organisation strategies and the plant configuration at low capital costs. Moreover, empirical data can be comparably easily obtained by the operation of small-scale systems and employed for the process modelling towards design and optimisation of large-scale units [10, 11]. However, the process performance of industrial-scale PSA/TSA systems can significantly differ from results obtained by the operation of a downsized pilot plant, mainly due to altered hydrodynamics and/or heat transfer conditions, which consequently influence the mass diffusion [12].

Taking into consideration the global demand for highly purified gases, the concept of pilot plant scale-up based on empirical and numerical research of a twin-bed PSA process for the generation of high-purity nitrogen is presented in this work. This technology is commercially established at product flow rates up to several thousand m^3_n/h (at 0 °C, 1 bar abs) and purity levels up to 10 ppm of the residual oxygen concentration. The kinetic separation of air is possible due to significantly faster adsorption of oxygen over nitrogen in PSA-plants equipped with carbon molecular sieves (CMS) [13]. Requirements and issues related to the pilot plant scale-up are presented and discussed. The numerical simulation of an industrial-scale twin-bed N_2-PSA plant is performed based on an experimentally verified mathematical model at different cycle times and product purity levels, proving an accurate estimation of both mass transfer kinetics and axial mass dispersion. An enhanced bed utilisation at extended mass transfer zone (MTZ) propagation along the adsorber length is exhibited. The numerical performance results obtained by simulation of units at different scales are compared and interpreted. Effects of the PSA scale-up factor, adsorber aspect ratio, packed-bed density, and flow resistances along the piping system on process performance at different product purity levels are presented and discussed. Demonstrated concepts can be applied to other separation processes carried out in corresponding PSA systems.

2 PSA scale-up essentials

The prospect of an accurate performance estimation of an industrial-scale PSA plant is based on combined experimental and numerical efforts. Specifically, relevant process simulations shall be performed by applying an experimentally validated mathematical model. For this purpose, empirical performance data ought to be collected while utilisation of the pilot plant which is a scaled-down version of the commercial system [14]. Furthermore, research under a broad range of operating conditions is substantial for understanding the system behaviour as the PSA performance depends on multiple process variables [8].

2.1 Mass dispersion

The first factor influencing the dissimilarity between the PSA performance obtained from the pilot- and the full-scale plant is the axial and/or radial mass dispersion, which refers to column geometry as well as gas velocity along the adsorber. Three main sources of dispersion arise during PSA operation; namely (1) gas channelling at the adsorber wall and/or in the kernel part of the packed-bed due to non-uniform interparticle voidage, (2) turbulent mixing of gas caused by flow disturbances around adsorbent pellets, and (3) molecular diffusion which occurs even in absence of a gas flow [15]. As the volume of the column increases, both the adsorbent-to-adsorber diameter ratio *d/D* and the surface-to-volume ratio of the fixed-bed *S/V* decline exponentially. Therefore, it is expected that large-scale adsorbers exhibit reduced dispersion effects and consequently improved performance figures in relation to the PSA pilot plants. Nevertheless, the challenge remains in finding an adequate mathematical representation of the mass dispersion originating from the three mentioned different sources when establishing the process model based on pilot plant data. It could be relatively misleading since mass dispersion and also mass transfer kinetics influence the formation of the mass transfer zone along the adsorber column. Hence, dispersion and/or mass transfer coefficients could be estimated erroneously, which would preclude the employment of the model for the design of industrial-scale units. Numerous studies, rules-of-thumb, and empirical correlations for the representation of mass dispersion in packed-beds are available and commonly acknowledged [16–21]. A summary of critical design parameters is presented in Table 1 [22]. The mathematical model of the PSA process shall include

Table 1 Critical adsorber design parameters, adapted [22]

Parameter	Comment
L/U	Critical
d	Critical
L/d	Minimal effect if it is larger than 150
L/D	Minimal effect if it is larger than 5
D/d	Minimal effect if it is larger than 20
Re	Minimal effect if it is larger than 10

all sources of dispersion that are relevant for actual flow and plant characteristics. Including insignificant dispersion relations in the model can result in substantially prolonged calculation time, making the design of industrial-scale units simply impractical. Particularly, the effect of radial dispersion can be omitted provided that the Reynolds number ($Re = \rho Ud/\mu$) remains larger than 10 and/or the ratio of adsorber length to adsorbent diameter (L/d) remains larger than 150. In such a case, the axial mass spreading becomes more significant than the radial mass spreading [12, 23]. Likewise, it is suggested that gas channelling effects become insignificant if the adsorber-to-adsorbent diameter ratio (D/d) is larger than 20 [24]. Usually, PSA pilot plants are designed in order to apply those correlations. It is crucial, however, to confirm that the scaled-up system exhibit the closest resembling flow and plant characteristics as were considered during PSA process modelling based on pilot plant data. Particular attention shall be put on maintaining the analogous packed-bed porosity which depends not only on adsorbent size and shape but also on the applied adsorber packing strategy [25].

2.2 Flow resistances

The second factor to be considered is the occurrence of multiple flow resistances caused by gas flowing through the adsorber and piping system. The pressure drop along the packed-bed results from the friction between gas and adsorbent pellets, in addition to the gravitational potential energy change due to the rising of the fluid [26]. The pressure drop magnifies as the adsorber length L is increased and/or the adsorbent-to-adsorber diameter ratio d/D is reduced [18]. For that reason, large-scale systems would exhibit abbreviated MTZ in comparison to pilot plants. Consequently, enhanced performance figures obtained from the operation of larger adsorbers are expected, as long as (1) the target operating pressure for the production and regeneration processes is yet attainable within the selected cycle time, and (2) the speed of pressurisation/depressurisation within the adsorber is not significantly inhibited. Otherwise, the elevated pressure drop along the packed-bed becomes a performance-limiting factor. The described fluid dynamic conditions are likewise dependent on the pressure drop across multiple plant mountings, i.e. pipes, fittings, control valves, bends, in-line filters, connectors, silencers, or adsorber column elements as perforated plates or sieves for the packed-bed support. For that reason, industrial-scale piping constituents characterised by flow coefficients Cv being in agreement with the pilot-plant equipment shall be selected, if possible. Moreover, significant discrepancies in the operation regimes of small-and large-scale shut-off vales ought to be foreseen. Solenoid valves, which are typically applied in small-scale PSA pilot plants, are able to perform the shut-off action within a range of milliseconds [27], minimising the flow resistance across the valve and allowing the execution of short steps within the PSA cycle. On the other hand, industrial-scale systems are usually equipped with pneumatically-operated rotary/butterfly valves [28]. Their response time corresponds to a few seconds, depending on the performance of the pneumatic actuator. Therefore, very often the PSA cycle organisation must be adapted for the design of large-scale units to meet those limitations. Since PSA performance strongly depends on flow resistances in the piping system, altered Cv coefficients could significantly contribute to inaccurate mathematical model predictions of the large-scale system performance [8].

2.3 Gas velocity

The third factor causing dissimilar operation regimes between pilot- and industrial-scale plants is usually an elevated superficial gas velocity within the adsorber column observed in larger PSA systems due to an increased throughput. When designing PSA plants, it is commonly accepted to limit the allowable gas velocity to less than 0.8 of the minimum fluidisation velocity during the production step, and to less than 1.8 of the minimum fluidisation velocity during the regeneration step [16]. Those requirements must be satisfied particularly during the PSA steps involving the rapid pressure change at both adsorber ends. By means of this strategy, the adsorbent attrition is most likely prevented, prolonging the lifespan of the material. In practice, to encounter those limitations, the aspect ratio of industrial-scale adsorber columns is typically adjusted to smaller values in comparison to those provided in pilot-plants. However, the proper engineering of the feed gas distribution system placed at the bottom of the column becomes more challenging as the adsorber diameter increases, which typically affects the capital costs.

2.4 Heat transfer

The fourth factor affecting differences between pilot- and large-scale PSA plants is related to dissimilar heat exchange conditions in the column. As the diameter of column D increases, the dissipation of heat generated due to adsorption

and compression is delayed. Consequently, the PSA performance of industrial-scale PSA units is reduced in relation to the pilot plant, due to diminished adsorption capacity at elevated operating temperatures. Consideration of this effect is indispensable when designing processes characterised by short PSA cycles and large values of adsorption enthalpy, which typically occurs in cases of gas separation on zeolites [29]. Therefore, large adsorbers would tend to operate under adiabatic conditions [30]. In order to ensure correctness of the mathematical model prediction, the heat transfer between pilot-scale adsorbers and environment shall be reduced by insulating columns prior to experimental research.

3 Experimental and numerical methods

Experimental data for the establishment of a mathematical model of high-purity nitrogen production are collected from a 2 × 2 L twin-bed PSA pilot plant. Two adsorbers are packed with a carbon molecular sieve of the type Shirasagi MSC CT-350. The unit is fed with dry compressed air. To control the product purity level, the product stream flow rate is adjusted. This control strategy represents the common operation of commercial plants. In the N_2-PSA technology, it is accepted that the product purity comprises the content of both nitrogen and argon since many industrial applications do not require an additional separation of inert gas mixtures. Consequently, the determination of the product purity is performed by assuming a binary gas mixture, where the difference to the oxygen concentration results in the nitrogen purity. The system structure resembles industrial-scale units; however, it is equipped with several ancillary detectors for sake of model development. A scheme of the twin-bed PSA pilot plant is presented in Fig. 1. Details of the unit, the adsorber column, and operating conditions are shown in Table 2.

The process comprises a six-step PSA cycle, which consists of (1) co-and counter-current bed pressure equalisation; (2) co-current pressurisation by feed with (3) counter-current backflow of the product; (4) production; (5) counter-current blow-down; and (6) counter-current purge by the product gas. The operation regime corresponds to the common operation of commercial PSA units. The flow rate of the counter-current purge equals in every experiment exactly 40% of the adsorber volume within the selected purge time. Details of the process organisation, supported by the scheme of a six-step cycle design, are described elsewhere [31]. The PSA performance indicators, productivity and air demand, are defined, determined, and verified according to the strategy described elsewhere [31].

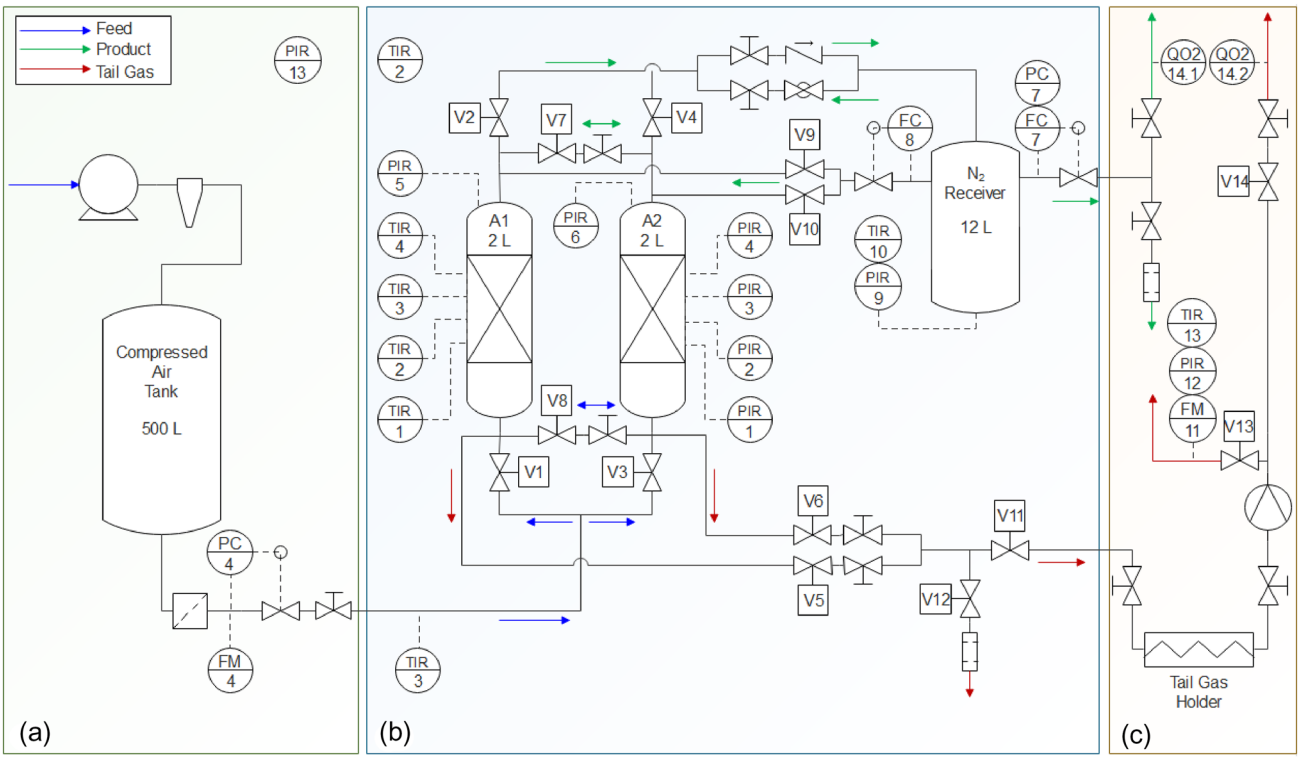

Fig. 1 Scheme of the PSA pilot-plant: **a** compressed air generation and pre-treatment, **b** twin-bed PSA unit, **c** gas analytics [31]

Table 2 Pilot plant details

Adsorbent type	Shirasagi MSC CT-350, cylindrical
Adsorbent pellet diameter [mm]	1.8
Packed-bed length [mm]	581
Packed-bed diameter [mm]	66
Packed-bed volume [L]	2 × 1.986
Filling bulk density [g/L]	711
Nitrogen receiver volume [L]	12
Internal diameter of piping system [mm]	6
Adsorption pressure [bar abs]	8
Operating temperature [°C]	20
Purge proportionality factor [%]	40
Equalisation time [s]	1
Equalisation strategy	Top/Top + Bottom/Bottom

The mathematical model of the process is established using the process simulator Aspen Adsorption™. Adsorbent packed-beds were discretised into 70 calculation nodes along their lengths. The quadratic differencing scheme (QDS) was selected to solve the set of differential equations coupled with algebraic equations. The feed gas is considered to be a two-component mixture of 20.9 vol.-% O_2 and 79.1 vol.-% N_2. The influence of operating conditions, cycle organisation, as well as plant design on the PSA process performance is validated by the agreement of experimental data and the outcome of dynamic process simulations [32]. Details of model development and its authentication are described elsewhere [33]. Model equations, a list of parameters, as well as adsorption equilibrium and kinetic data, are given in the supplementary information. The simulation data presented in this work are obtained at cyclic-steady-state (CSS) conditions; namely, when the gas composition in the product stream does not vary in time [34–36]. The number of cycles necessary to reach the CSS state depends on the required product purity level as well as the composition of gas accumulated in the N_2-receiver tank at the starting point of the process.

4 Results and discussion

4.1 Model applicability for scaled-up plants

The employment of the developed mathematical model based on a pilot-plant outcome for the design of industrial-scale units can be assessed by consideration of process performance data at different cycle conditions. In this case, the half-cycle time is considered. The success of a quantitative prediction of the PSA performance lies in the accurate prediction of the breakthrough curve of the adsorber. An agreement of empirical and numerical results indicates the reliable estimation of both mass transfer kinetics as well as mass dispersion in the studied system since both factors primarily influence the shape of the breakthrough curve. Moreover, the consideration of different half-cycle times allows insight into the PSA operation at various bed utilisations which would correspond to the operation of units at different magnitudes. By means of this strategy, the development of MTZ along the adsorber column can be simulated and the formation of the concentration front can be examined, because a relatively good agreement among experimental and simulated temperature profiles is achieved, as shown in Fig. 2.

Empirical and numerical performance indicators of high-purity N_2-PSA at different half-cycle times are presented in Fig. 3. Independent from the purity level, the dynamic simulation predicts qualitatively well productivity and air demand. A slight imprecision in quantitative estimation of performance data occurs only on the highest investigated purity level of 10 ppm O_2, which could most likely be caused by inaccuracy in the estimation of adsorption isotherms at very low oxygen partial pressure [33] and/or measurement uncertainty at very low oxygen concentration [31]. The effect of the PSA half-cycle time on the nitrogen productivity greatly depends on the required product purity. On one hand, shorter cycles enlarge productivity at low purity levels (> 100 ppm O_2 in product stream) by preventing premature column breakthrough due to enhanced channelling effects promoted by relatively large gas superficial velocity. On the other hand, longer cycles allow extended gas residence time in the adsorber column which improves the gas separation efficiency at high purity levels (< 10 ppm O_2 in product stream). Since the variation of the half-cycle time changes the time span proportion of pressurisation and production steps, the air demand increases as the half-cycle time is reduced at every investigated product purity level due to a smaller amount of compressed air utilised for the production purpose [8].

Numerical breakthrough curves at different half-cycle times are presented in Fig. 4. Given that the final product purity corresponds to the integral average value of the oxygen concentration within the PSA cycle, the maximum allowable product contamination level detected at the end of the production step depends on the selected half-cycle time. Since the dynamic simulation corresponds to the operation of practical PSA systems, it can be seen that at every investigated product purity level the breakthrough curve does not begin at the zero-level of oxygen

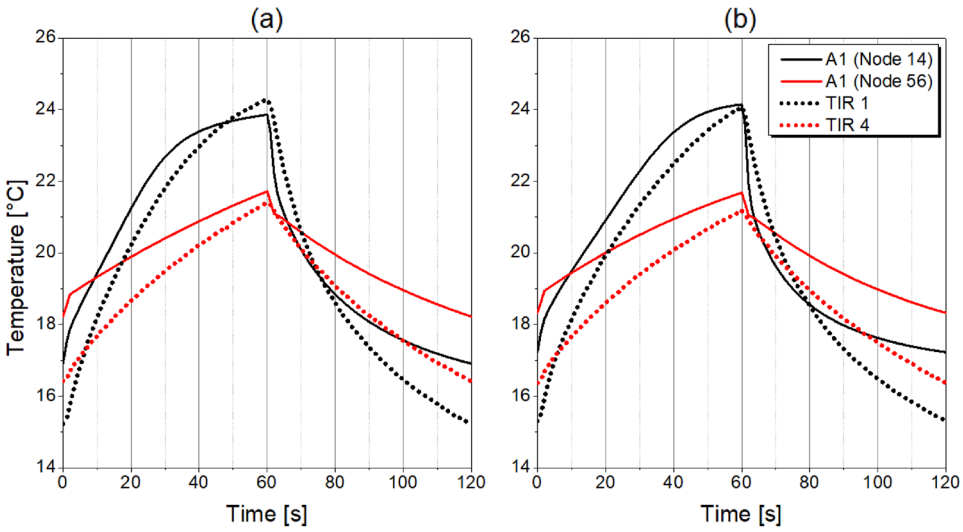

Fig. 2 Experimental (dotted line) and simulated (solid line) temperature profiles at selected positions of the adsorber during the PSA cycle: **a** at product purity of 1000 ppm O_2, **b** at product purity of 10 ppm O_2 [33]

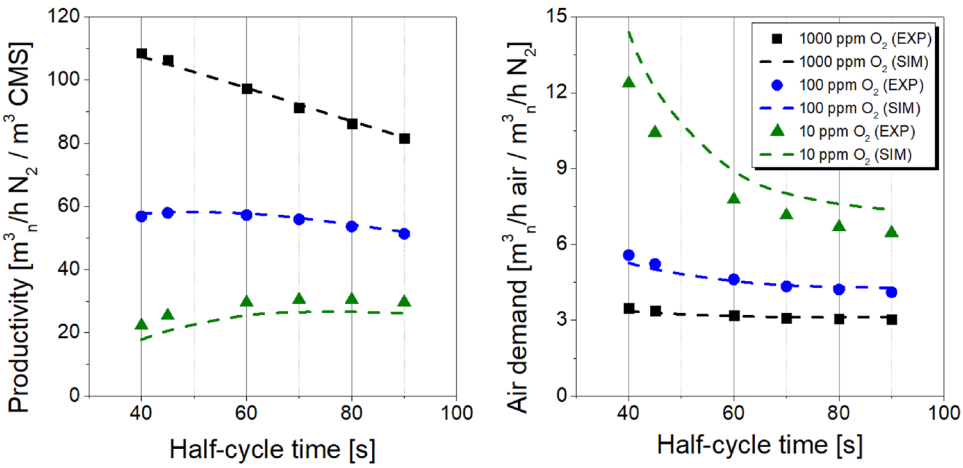

Fig. 3 Experimental and simulated PSA performance indicators at different half-cycle times

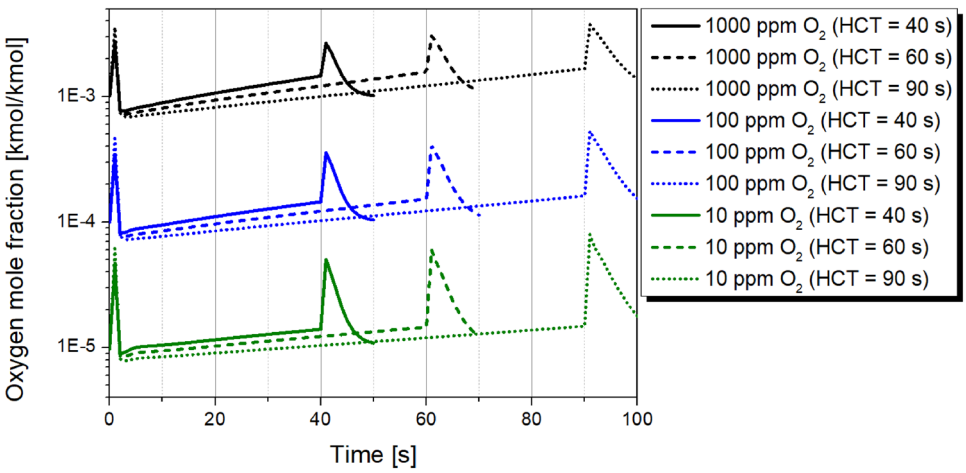

Fig. 4 Simulated PSA break-through curves at different half-cycle times

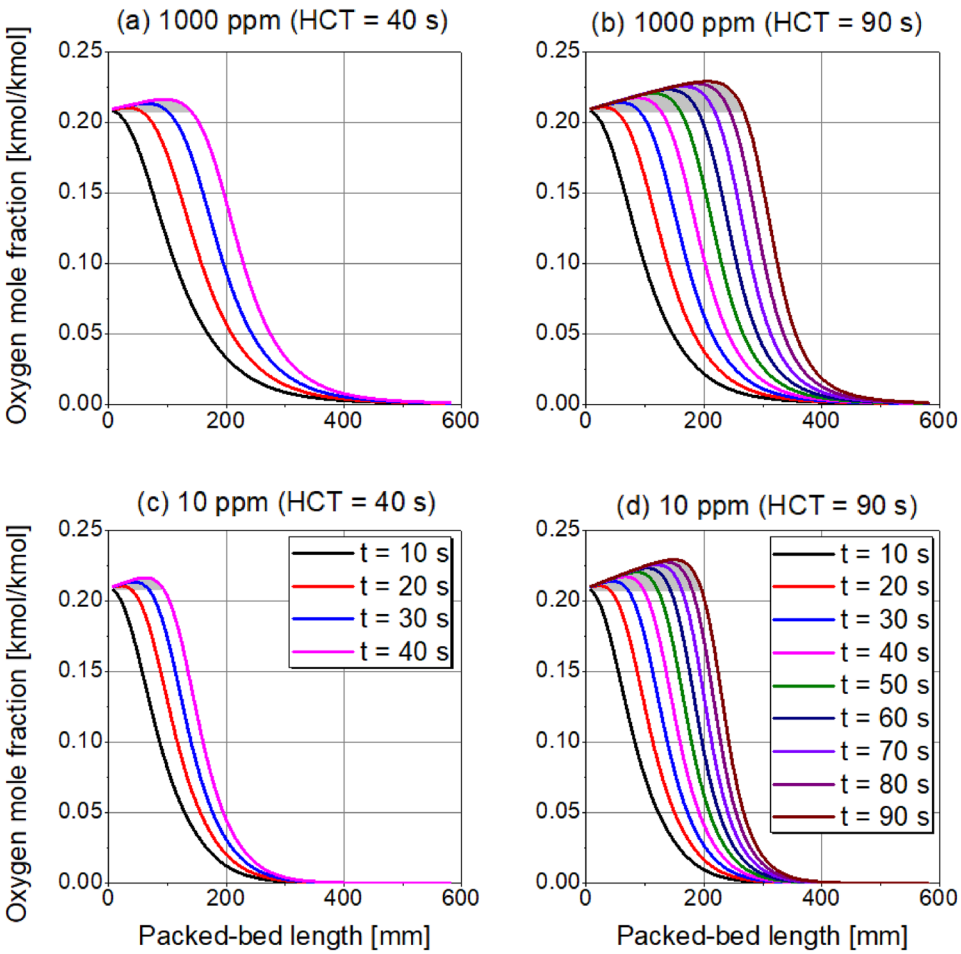

Fig. 5 Simulated oxygen mass transfer zone at different half-cycle times

concentration. Therefore, the MTZ propagates through the entire adsorber length, which is shown in Fig. 5.

An extended MTZ along the adsorber occurs at low purity levels, indicating an enhanced mass dispersion caused by the elevated gas superficial velocity. In contrast, at high nitrogen purity levels, the MTZ is situated mostly at the bottom part of the bed; therefore, the top part is occupied almost exclusively by purified nitrogen. As a result of the type-I isotherm describing the equilibrium in the studied system [33], at all investigated process conditions, the oxygen concentration front is self-sharpening in the initial phase of the production step and approaches a constant pattern behaviour as the half-cycle time is increased. Whereas at thermodynamic equilibrium both components are adsorbed by the CMS in a similar quantity, a roll-up effect occurs which indicates a dominant adsorption of nitrogen over oxygen due to its higher concentration in the feed stream. Therefore, both factors, the shape of concentration front propagation and the magnitude of the roll-up effect, would eventually have an impact on the bed utilisation. The velocity of selected oxygen concentration levels U_y of 0.15 and 0.05 kmol/kmol at different adsorption duration t and the extend of the roll-up effect χ, indicated by a grey area in Fig. 5, are presented in Table 3. The bed utilisation φ is calculated by a numerical integration according to Eq. 1, where: y—oxygen mole fraction [kmol/kmol], y_{in}—oxygen mole fraction in inlet stream which equals 0.209 kmol/kmol, L—packed-bed length [mm], L_{max}—total packed-bed length which equals 581 mm. The extend of the roll-up effect χ is calculated by a numerical integration according to Eq. 2, where L_{yin}—packed-bed length at which oxygen mole fraction refers to the inlet stream.

$$\varphi = \frac{\int_0^{L_{\max}} y(L)_{t=HCT} dL - \chi}{L_{\max} \cdot y_{in}} \tag{1}$$

$$\chi = \int_0^{L_{y_{in}}} y(L)_{t=HCT} dL - L_{y_{in}} \cdot y_{in} \tag{2}$$

The constant pattern behaviour does not occur in the studied system even at prolonged adsorption duration since higher concentration levels propagate faster in relation to

Table 3 MTZ analysis at different half-cycle times, based on numerically obtained data

	1000 ppm O_2				10 ppm O_2			
	HCT = 40 s		HCT = 90 s		HCT = 40 s		HCT = 90 s	
Productivity (SIM) [m^3_n/h N_2/m^3 CMS]	107.40		81.91		17.87		26.19	
Air demand (SIM) [m^3_n/h air/m^3_n/h N_2]	3.358		3.134		14.395		7.364	
χ[kmol/kmol mm]	0.6321		3.2240		0.4164		2.3734	
φ [%]	41.62		57.50		28.88		42.67	
t [s]	$U_{0.15}$ [mm/s]	$U_{0.05}$ [mm/s]	$U_{0.15}$ [mm/s]	$U_{0.05}$ [mm/s]	$U_{0.15}$ [mm/s]	$U_{0.05}$ [mm/s]	$U_{0.15}$ [mm/s]	$U_{0.05}$ [mm/s]
10	4.61	3.91	4.13	3.60	3.15	2.65	3.22	2.74
20	3.92	3.57	3.51	3.05	2.49	2.10	2.62	2.22
30	3.55	3.13	3.17	2.75	2.16	1.82	2.30	1.94
40			2.92	2.57			2.08	1.78
50			2.72	2.40			1.90	1.62
60			2.55	2.28			1.74	1.49
70			2.40	2.17			1.60	1.41
80			2.27	2.05			1.48	1.29

lower concentration levels at all investigated process conditions. Therefore, the self-sharpening MTZ results in a larger bed utilisation at longer cycle times despite an intensified nitrogen adsorption associated with the roll-up effect. Moreover, it can be noticed that a faster propagation of concentration profiles results in an increased nitrogen productivity at both studied levels of product purity, which indicates an enhanced kinetic selectivity of the CMS in respect to the air components.

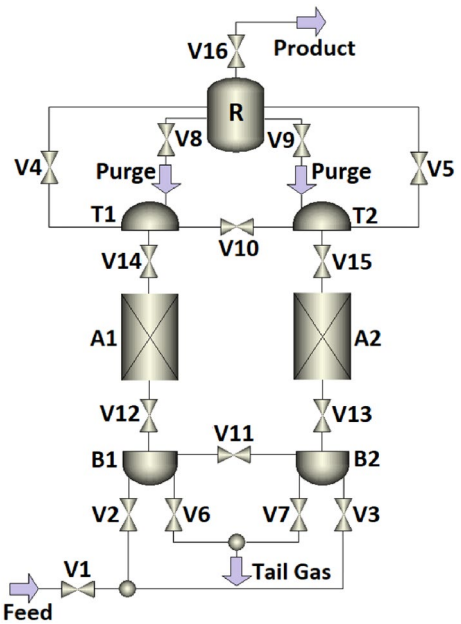

Fig. 6 Flow sheet of the twin-bed PSA created in the simulation software Aspen Adsorption™ [33]

Considering that (1) the mathematical model accurately predicts the PSA performance at various half-cycle times and thus proving the correct estimation of both axial mass dispersion and mass transfer kinetics at various product purity levels, and (2) a further propagation of MTZ along the adsorber leads to an improved bed utilisation, the dynamic simulation of units in industrial dimensions can be performed as long as the process conditions are corresponding.

4.2 PSA performance at different scale-up factors

The scheme of the PSA system implemented in the process simulator is presented in Fig. 6. The numerical investigation of the performance at different scale-up factors α was executed by a proportional increase of (1) volume of packed-beds V_{A1} and V_{A2}, (2) volume of nitrogen receiver V_R, (3) volume of top and bottom adsorbers voids V_T and V_B, (4) Cv coefficients of selected valves V, and (5) purge stream flow rate F_{purge}. Applied values are given in Tables 4 and 5. By means of this strategy, the adsorber column geometry as

Table 4 Cv coefficients at different scale-up factor α

α [-]	Cv [kmol/s/bar]				
	V1	V2, V3	V10, V11	V12, V13	V14, V15
1	5.00E−01	9.00E−04	2.50E−05	1.10E−04	9.50E−04
5	2.50E+00	4.50E−03	1.25E−04	5.50E−04	4.75E−03
25	1.25E+01	2.25E−02	6.25E−04	2.75E−03	2.38E−02
100	5.00E+01	9.00E−02	2.50E−03	1.10E−02	9.50E−02
500	2.50E+02	4.50E−01	1.25E−02	5.50E−02	4.75E−01
2000	1.00E+03	1.80E+00	5.00E−02	2.20E−01	1.90E + 00

Table 5 PSA configuration at different scale-up factor α

α [-]	V_{A1}, V_{A2} [L]	L/D [-]	D [mm]	L [mm]	V_R [L]	F_{purge} [m^3_n/h]	V_{B1}, V_{B2} [cm^3]	V_{T1}, V_{T2} [cm^3]
1	1.99	8.8	66	581	12	0.0484	18.5	35.0
5	9.93	8.8	113	993	60	0.2419	92.4	175.0
25	49.65	8.8	193	1698	300	1.2096	461.8	875.0
100	198.60	8.8	306	2696	1200	4.8384	1847.0	3500.0
500	993.01	8.8	524	4610	6000	24.1920	9235.0	17,500.0
2000	3972.04	8.8	832	7318	24000	96.7680	36,940.0	70,000.0

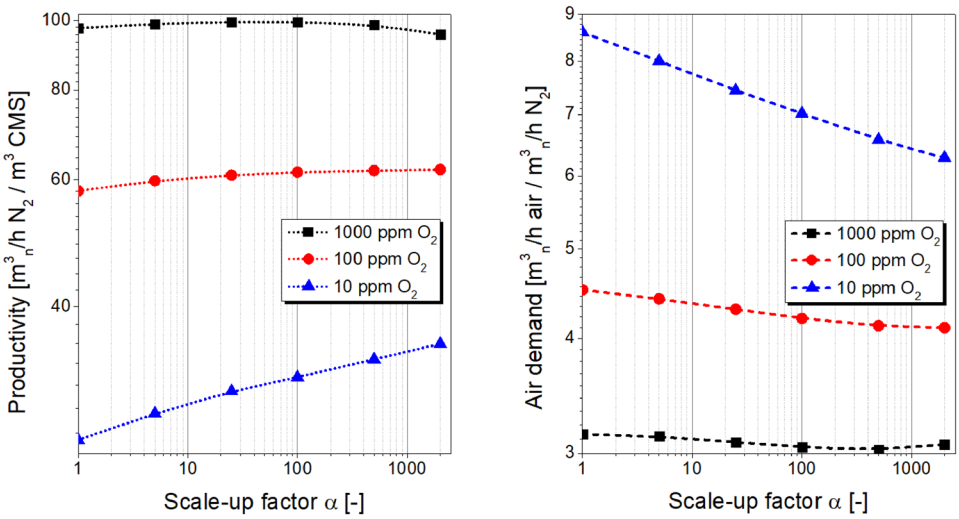

Fig. 7 Simulated PSA performance at different scale-up factors α

well as flow resistances are corresponding to the pilot-plant, enabling a systematic study of the system behaviour. Here, the HCT equals 60 s at all investigated process conditions. Operating temperature, adsorption pressure, and the equalisation method refer to the data presented in Table 2. The sensitivity study exhibited no substantial variation in dynamic simulation results at increased number of calculations nodes. Therefore, the number of calculation nodes is not altered and equals 70 at all investigated process conditions to avoid an extended computation time.

The PSA performance results at different scale-up factors are displayed in Fig. 7.

The effect of the plant scale-up factor α on PSA performance indicators strongly depends on the required product purity. When generating the product at low purity levels ($\geq$ 1000 ppm O_2), both productivity and air demand values remain rather insensitive to the PSA system enlargement. It is observed that the nitrogen productivity increases by scaling-up the system up to an α-value of about 100, which indicates reduced mass axial dispersion effects as the adsorbent-to-adsorber diameter ratio d/D is reduced. At $\alpha = 100$, the productivity is enlarged by about 2% in relation to the pilot-plant operation. At larger values of scale-up factor ($\alpha > 100$), the effect of axial mass dispersion becomes irrelevant; however, the productivity decreases due to an extended pressure drop along the packed-bed, which disables the proper adsorbent regeneration, as shown in Fig. 8. The minimum value of the air demand is observed at $\alpha = 500$, indicating the highest bed utilisation.

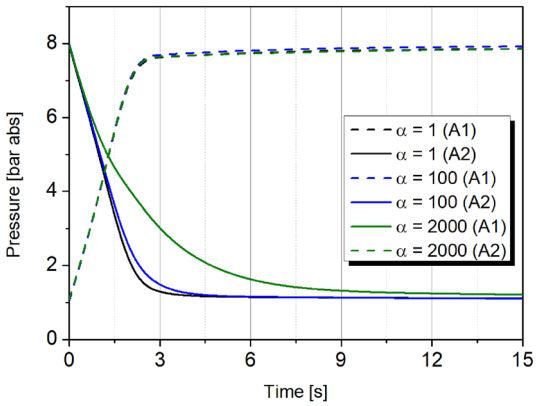

Fig. 8 Simulated pressure profiles at the top of adsorber columns A1 and A2 during the initial phase of the PSA cycle at different scale-up factors α

When generating the product at high purity levels ($\leq$ 100 ppm O_2), the productivity increases and the air demand decreases as the system approaches the

industrial-scale. Especially at the highest investigated nitrogen purity level (10 ppm O_2), the enlargement of the PSA system by the factor of 2000 results in a productivity increase of about 36%, and the air demand reduction of about 27% in relation to the pilot-plant operation. In this case, the elevated flow resistance during the counter-current depressurisation proves to not be a limiting factor, as the relatively condensed oxygen mass transfer zone is situated mostly in the bottom part of the bed. Therefore, an increased pressure drop along the packed-bed inhibits the evacuation of the purified nitrogen accumulated in the top part of the column. Hence, it is strongly recommended to utilise larger PSA pilot plants for investigating high-purity nitrogen production in order to gain more reliable design data.

In the industrial practice, the particular scale-up factor of top and bottom adsorber voids does not necessarily grow closely with the general scale-up factor α. In this case, it is expected that a provision of smaller void volumes would result in reduced air demand figures without a significant impact on the productivity [8, 37]; provided that wall effects and gas channeling are insignificant for the considered adsorber geometry, i.e. $L/D > 5$ and $D/d > 20$. Otherwise, a notable effect of void volumes on PSA performance would be expected, especially as the required product purity level increases, regardless of the plant size.

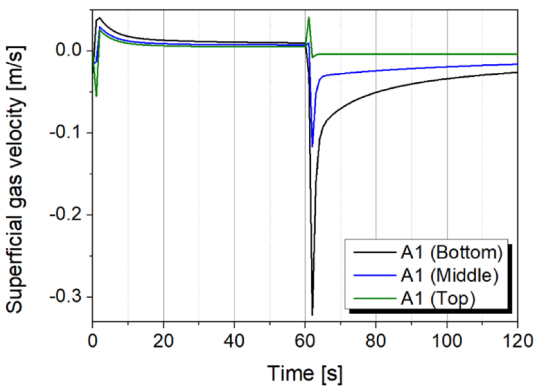

Fig. 9 Simulated gas velocity during the PSA cycle at different scale-up factor α; here time ranges of 0–60 s and 60–120 s indicate production and regeneration steps, respectively

Furthermore, it is clear that the allowable gas velocity during the regeneration step becomes a limiting factor during the design of industrial-scale PSA systems. To assess whether the simulated processes could be applied in practice, an analysis of the gas velocity during the PSA cycle is be performed. The development of the gas velocity formed during the operation of the PSA pilot plant ($\alpha = 1$) at different column heights is presented in Fig. 9. The highest amplitudes of the gas velocity are detected at the bottom of the adsorber during the pressure equalisation step, as well as at the beginning of production and regeneration steps. Those extremum values of the gas velocity shall be compared to the minimum fluidisation velocity determined at the same time in order to verify the hydrodynamic constraints of the system. The determination of the minimum fluidisation velocity U_f is based on the Ergun pressure drop equation. No significant difference in the minimum fluidisation velocity at different column heights was detected. The ratio of the actual gas velocity to the minimum fluidisation velocity at different scale-up factors α during the nitrogen production at 1000 ppm O_2 purity level is presented in Table 6. An additional sensitivity study exhibited no substantial variation in values of the gas velocities along the column at different product purity levels; however, the production of low-purity nitrogen is associated with fairly higher values of the gas velocity in relation to the high-purity nitrogen generation.

Taking into consideration the hydrodynamic limitations of the system during the counter-current regeneration step ($U/U_f \leq 1.8$), it is proved that the employed scale-up strategy is valid up to the scale-up factor α equal to about 7.5. A further increase of the adsorber volume is not recommended. Thus, as long as the design of larger PSA units is considered, other scale-up approaches shall be examined and verified.

4.3 PSA performance at different aspect ratios

Provided that the gas velocity shall be reduced in order to encounter the hydrodynamic limitations of the system, a very common practice is the adjustment of the adsorber aspect ratio to lower values. Moreover, the size of industrial PSA systems is commonly restricted by the available space indoors or outdoors. Hence, very often the

Table 6 Simulated gas velocities at different scale-up factors α, during the nitrogen production at 1000 ppm O_2 purity level

α [-]	Production step			Regeneration step		
	U [m/s]	U_f [m/s]	U/U_f [-]	U [m/s]	U_f [m/s]	U/U_f [-]
1	0.04	0.19	0.21	− 0.32	− 0.34	0.95
5	0.07	0.19	0.36	− 0.55	− 0.34	1.64
25	0.11	0.19	0.59	− 0.97	− 0.34	2.89
100	0.18	0.26	0.71	− 1.61	− 0.33	4.87
500	0.37	0.26	1.43	− 2.71	− 0.33	8.25
2000	0.69	0.26	2.65	− 3.49	− 0.34	10.41

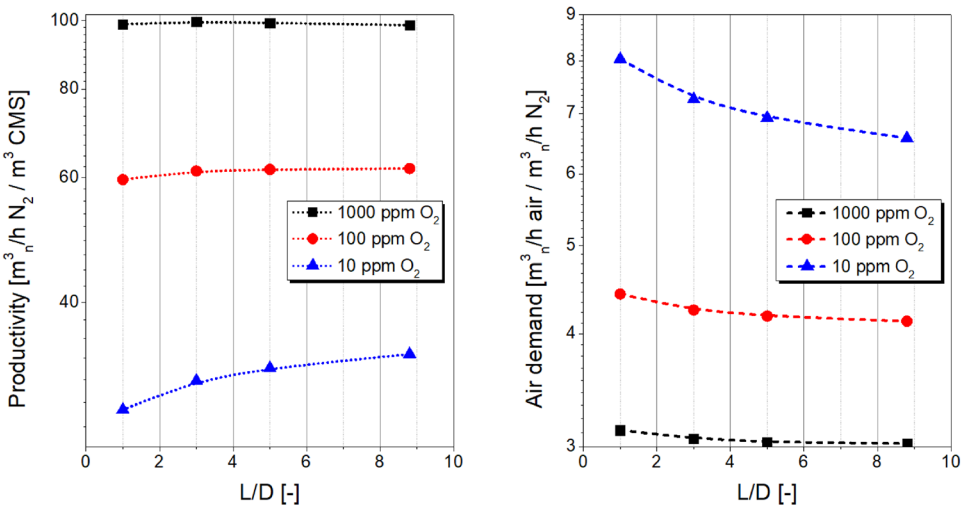

Fig. 10 Simulated PSA performance at different adsorber aspect ratios

L/D ratio of adsorbers is adjusted to meet those requirements. For that reason, a systematic study of the effect of the *L/D* ratio on the PSA performance was conducted. Dynamic simulations were executed at the PSA scale-up factor equal to 500; therefore, in this case, the volume of a single packed-bed equals about 993 L. Other operating conditions of the process refer to those applied in the previous section. The results are presented in Fig. 10.

The nitrogen productivity remains rather insensitive to the variation of the *L/D* ratio, especially at low product purity levels ($\geq$ 100 ppm O_2). Nonetheless, at all investigated process conditions, the increased *L/D* ratio results in lower air demand values, as the impact of mass axial dispersion along the adsorber length is diminished. However, the effect proves to be rather insignificant as the required product purity level decreases. Therefore, utilisation of adsorber columns with large *L/D* ratios is recommended exclusively when high purity nitrogen ($\leq$ 10 ppm O_2) is required, mostly due to the substantial air demand reduction.

The considerable effect of the adsorber aspect ratio on the gas velocity is presented in Table 7. As expected, the gas velocity is significantly reduced at a lower *L/D* value. It is proved that the presented industrial-scale PSA process could be implemented in practice at the *L/D* ratio equal to 1, as long as the process conditions are corresponding. In this case, the hydrodynamic limitations of the system are not compromised.

4.4 PSA performance at different packed-bed density

Differences among process performance figures obtained during the operation of PSA plants at different magnitudes could as well arise from the execution of dissimilar adsorber packing strategies, which results in the variation of the packed-bed density ρ_{bed} and packed-bed porosity ϵ_{bed} characteristics. Whereas the packed-bed density of small-scale columns can be somehow elevated by the employment of alternative packing methods and their combinations, i.a. tapping, vibrating, snowstorm filling; the industrial-scale adsorbers are filled almost exclusively (1) by the snowstorm filling method if adsorbers are equipped with top flanges, or (2) by the standard flow-pack method if adsorbers are equipped only with an inlet nozzle. All efforts invested to increase the packed-bed density lead to an elevated adsorption capacity of the system, as well as to lower porosity of the packed-bed and a reduction of mass dispersion effects. The results of sensitivity studies concerning the effect of packed-bed density ρ_{bed} on PSA performance at different plant scale-up factors and adsorber aspect ratios are presented in Fig. 11. The selected range of the packed-bed density corresponds to the information provided in the adsorbent data sheet. The

Table 7 Simulated gas velocities at different *L/D* ratios, during the nitrogen production at 1000 ppm O_2 purity level

L/D [-]	Production step			Regeneration step		
	U [m/s]	U_f [m/s]	U/U_f [-]	U [m/s]	U_f [m/s]	U/U_f [-]
1	0.07	0.19	0.39	− 0.60	− 0.34	1.79
3	0.15	0.25	0.59	− 1.32	− 0.33	3.97
5	0.22	0.26	0.86	− 1.92	− 0.33	5.85
8.8	0.69	0.26	2.65	− 3.49	− 0.34	10.41

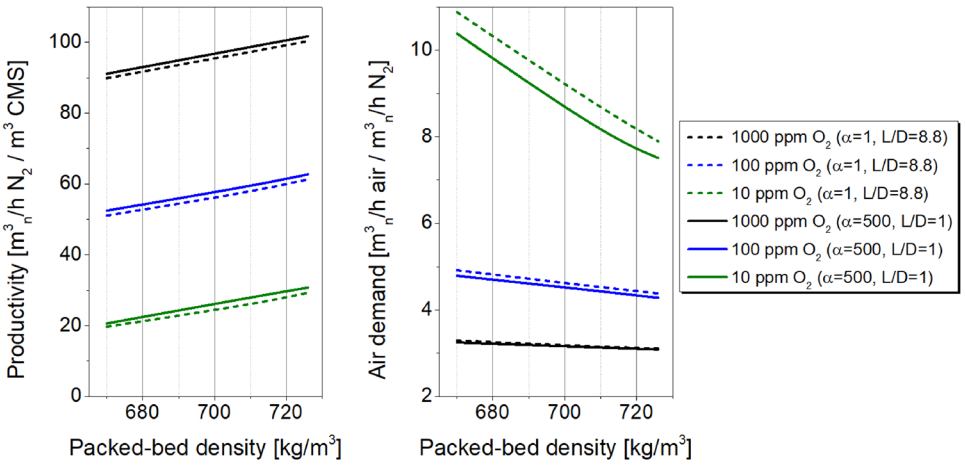

Fig. 11 Simulated PSA performance at different packed-bed density

packed-bed porosity ε_{bed} was calculated according to Eq. 3, based on the experimentally determined value of adsorbent apparent density ρ_{app}, which equals 1193.12 kg/m^3.

$$\varepsilon_{bed} = 1 - \frac{\rho_{bed}}{\rho_{app}} \tag{3}$$

At all investigated process conditions, the elevated packed-bed density results in a linear increase in productivity figures. The increment of the adsorber packed-bed density by about 8% causes an enlargement of the nitrogen productivity of about 12%, 20%, and 49% at product purity levels of 1000 ppm O_2, 100 ppm O_2, and 10 ppm O_2, respectively, regardless the adsorber volume or aspect ratio. Furthermore, the air demand decreases predominantly linearly with the elevation of packed-bed density at all investigated process conditions. This effect becomes more significant as the product purity increases. The enlargement of the adsorber packed-bed density by about 8% causes the air demand reduction of about 5%, 11%, and 27% at product purity levels of 1000 ppm O_2, 100 ppm O_2, and 10 ppm O_2, respectively.

4.5 Validation of the industrial-scale PSA simulations

In order to confirm that the mathematical model can be utilised for the design of large-scale PSA systems, the experimental performance results obtained during the operation of an industrial twin-bed N_2-PSA plant equipped with the same adsorbent are compared to the outcome of dynamic simulations at the corresponding process conditions. The properties of the industrial-scale PSA system are presented in Table 8. The experimental data were provided by SysAdvance©, Portugal.

Table 8 Properties of the industrial-scale twin-bed N_2-PSA system

Packed-bed length [mm]	1848
Packed-bed diameter [mm]	1200
Packed-bed aspect ratio [-]	1.54
Packed-bed volume [L]	2089
Filling bulk density [g/L]	650
Packed-bed porosity [-]	0.4
Purge stream flow rate [m^3_n/h]	60.2
Adsorber bottom void volume [L]	766
Adsorber top void volume [L]	145
N_2-receiver tank volume [L]	5000
Feed pressure [bar abs]	11.3
Production pressure [bar abs]	10.7
Operating temperature [°C]	20
Duration of production step [s]	50
Duration of regeneration step [s]	50
Duration of equalisation step [s]	6
Equalisation strategy	Top/Top + Bottom/Bottom
Cycle time [s]	112
Product purity [ppm O_2]	837
Product flow rate [m^3_n/h N_2]	485.0
Productivity [m^3_n/h N_2/m^3 CMS]	116.1
Air demand [m^3_n/h air/m^3_n/h N_2]	Unknown

Taking into consideration the volume of the large-scale adsorber, it can be deduced that a pilot-plant scale-up factor $\alpha = 1052$ would apply in this case. However, the dynamic simulation was adapted to correctly simulate the functioning of industrial-scale shut-off valves installed in the system. Therefore, *Cv* coefficients were arbitrarily adjusted, predominantly to smaller values in relation to those implemented for the simulation of pilot-plant behaviour, multiplied by a factor of 1052. Moreover, in certain cases, a linear increase of *Cv* values was implemented, in order to account for a

Table 9 *Cv* coefficients applied for the simulation of the industrial-scale PSA system

		Cv [kmol/s/bar]						
		V1	V2, V3	V4, V5	V6, V7	V10, V11	V12, V13	V14, V15
$\alpha = 1052$		5.26E+02	9.47E−01	–	–	2.63E−02	1.16E−01	9.99E−01
Adapted values	Initial	1.00E+01	5.00E−03	5.00E−03	2.00E−02	1.00E−03	2.02E−01	3.00E−02
	Final	1.00E+01	1.50E−01	1.50E−01	1.50E−01	8.00E−03	2.02E−01	3.00E−02
	Ramp [*Cv*/s]	–	0.0029	0.0029	0.0026	0.0012	–	–

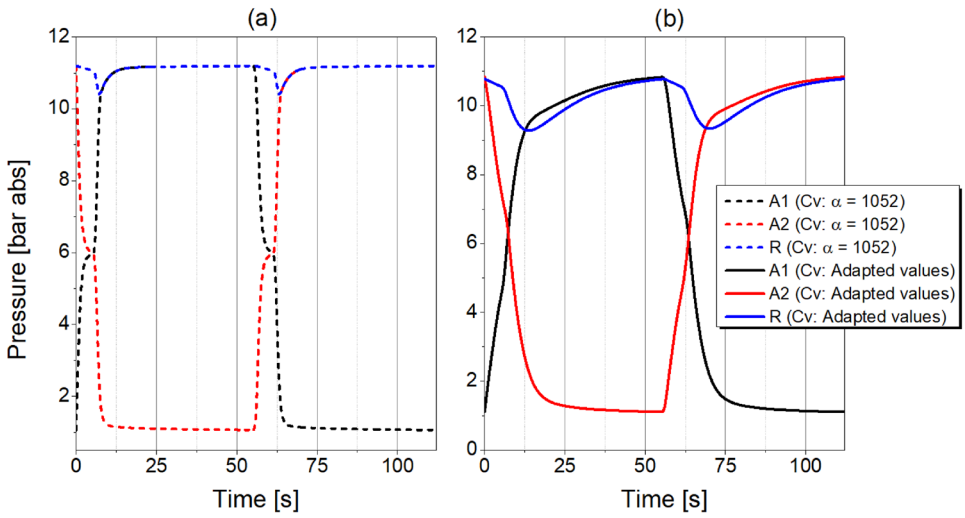

Fig. 12 Simulated pressure profiles during the operation of industrial-scale PSA unit: **a** *Cv* coefficients according to the pilot plant, multiplied by a scale-up factor of 1052; **b** *Cv* coefficients adapted to reflect behaviour of large-scale PSA systems

Table 10 Simulated performance of an industrial-scale PSA system

	Cv ($\alpha = 1052$)	*Cv* (adapted values)
Product purity [ppm O_2]	837	837
Productivity (SIM) [m^3_n/h N_2/m^3 CMS]	72.4	115.8
Air demand (SIM) [m^3_n/h air/m^3_n/h N_2]	4.25	4.05
Inaccuracy of productivity prediction [%]	**− 37.7**	**− 0.3**
U/U_f [-] (Production step)	1.32	0.45
U/U_f [-] (Regeneration step)	4.11	1.13

prolonged response time of industrial-scale shut-off valves, which tend to operate analogously to actuators. The comparative valve coefficients *Cv* are shown in Table 9. By means of this strategy, the pressure swing is not achieved as rapidly as when utilising pilot-scale units, as presented in Fig. 12, which resembles a realistic operation regime of large-scale PSA plants. If possible, the validation of generated pressure curves presented in Fig. 12b with experimental data is strongly recommended to verify whether *Cv* values are adjusted correctly.

Simulation results of the industrial-scale PSA are shown in Table 10. The presented outcome clearly demonstrates the significance of the proper estimation of flow resistances along the piping system for accurate prediction of the unit performance. When implemented values of *Cv* coefficients simply scaled-up by the factor α, the mathematical model underestimates the productivity by nearly 38%. In this case, very rapid pressurisation and depressurisation at the beginning of the PSA cycle, as shown in Fig. 12a, give rise to an excessive gas velocity along the adsorber, which surpasses the hydrodynamic limitations of the system. Moreover, the production pressure does not correspond to the experimental value, as reported in Table 8.

On the other hand, when the implemented *Cv* coefficients are adapted to simulate pragmatic pressure profiles, observed during the operation of large-scale systems, as shown in Fig. 12b, the mathematical model predicts the PSA productivity with inaccuracy smaller than 1%. Furthermore, as reported in Table 10, the ratio of the gas velocity to the minimum fluidisation velocity falls within the recommended range for the operation of packed-bed reactors. In this case, reduced pressurisation and depressurisation rates result in significantly smaller oxygen concentration amplitudes, observable on the oxygen breakthrough curve during the pressure equalisation step, as well as at the beginning of production and regeneration steps, as presented in Fig. 13. Thus, increased flow resistances along the piping system reduce the driving force for the desorption process at the time of the adsorber depressurisation, which results in the

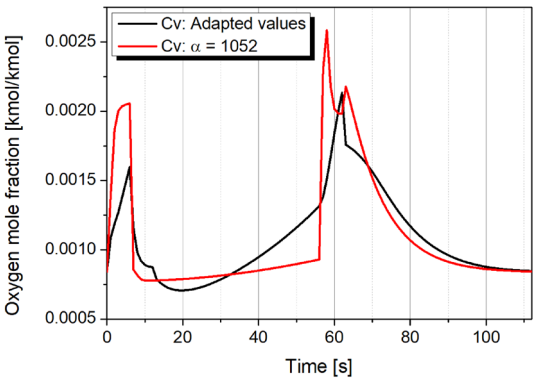

Fig. 13 Simulated oxygen breakthrough curves during the industrial-scale PSA cycle; here time ranges 0–6 s, 6–56 s, 56–62 s, and 62–112 s indicate equalisation, production, equalisation, and regeneration steps, respectively

minor transfer of the highly oxygen-enriched gas into the neighbour column. For that reason, the adsorption capacity in the subsequent production step is larger for the process with adapted *Cv* coefficients in relation to the process with straightforwardly scaled-up *Cv* values. Thereby, an increased nitrogen productivity is obtained. Moreover, a slightly lower air demand was identified when adapted *Cv* coefficients are implemented in the process simulator, pointing out the improved bed utilisation at the same product purity level.

5 Conclusions

The developed mathematical model based on pilot-scale high-purity twin-bed N_2-PSA experiments can be utilised for the design of industrial-scale systems provided that (1) the pilot-plant construction closely resembles an industrial-scale unit, (2) the mathematical model is developed in accordance with dimensions of considered packed-bed as well as adsorbent particles, and (3) the process performance obtained during the operation of the pilot-plant at different cycle times and product purity levels is predicted quantitatively correctly by the dynamic simulations, proving an accurate estimation of both mass transfer kinetics and axial mass dispersion. It is demonstrated that large-scale PSA units can be designed by the employment of scale-up factors or the adjustment of the adsorber aspect ratio, as long as hydrodynamic limitations of the system are respected. Moreover, it is proved that the proper estimation of packed-bed density, as well as the adjustment of flow resistances in the PSA piping system, become crucial aspects of an accurate prediction of the PSA plant performance. Additionally, it is proved that the size of pilot plants erected for a direct access to PSA design data at high product purity levels shall be significantly bigger than for low-purity applications.

Supplementary Information The online version contains supplementary material available at https://doi.org/10.1007/s10450-023-00382-2.

Acknowledgements The authors thank CarboTech AC GmbH, Essen, Germany, for provisioning of CMS utilised in the PSA pilot plant for the experimental research; as well as SysAdvance, Póvoa de Varzim, Portugal, for providing experimental process performance data collected from an industrial-scale PSA unit. Moreover, we also thank Dr. Armin D. Ebner from the University of South Carolina, Columbia, SC, for his valuable comments on the topic, supported by his experience in the design of industrial-scale PSA systems. Muenster University of Applied Sciences is thanked for respectable project grants.

Funding Open Access funding enabled and organized by Projekt DEAL.

Declarations

Conflict of interest The authors certify that there is no actual or potential conflict of interest in relation to this article.

References

1. Jiang, L., Wang, R.Q., Gonzalez-Diaz, A., Smallbone, A., Lamidi, R.O., Roskilly, A.P.: Comparative analysis on temperature swing adsorption cycle for carbon capture by using internal heat/mass recovery. Appl. Therm. Eng. **169**, 114973 (2020)
2. Raganati, F., Chirone, R., Ammendola, P.: CO2 capture by temperature swing adsorption: working capacity as affected by temperature and CO2 partial pressure. Ind. Eng. Chem. Res. **59**, 3593–3605 (2020)
3. Salazar Duarte, G., Schürer, B., Voss, C., Bathen, D.: Adsorptive Separation of CO2 from flue gas by temperature swing adsorption processes. CBEN **4**, 277–288 (2017)
4. Shang, J., Hanif, A., Li, G., Xiao, G., Liu, J.Z., Xiao, P., Webley, P.A.: Separation of CO2 and CH4 by pressure swing adsorption using a molecular trapdoor chabazite adsorbent for natural gas purification. Ind. Eng. Chem. Res. **59**, 7857–7865 (2020)
5. Wurzbacher, J.A., Gebald, C., Steinfeld, A.: Separation of CO2 from air by temperature-vacuum swing adsorption using diamine-functionalized silica gel. Energy Environ. Sci. **4**, 3584 (2011)
6. Zhan, G., Bai, L., Zeng, S., Bai, Y., Su, H., Wu, B., Cao, F., Shang, D., Li, Z., Zhang, X., Zhang, S.: Dynamic process simulation and assessment of CO_2 removal from confined spaces using pressure swing adsorption. Ind. Eng. Chem. Res. **59**, 16407–16419 (2020)

7. Chen, Y.-F., Lin, P.-W., Chen, W.-H., Yen, F.-Y., Yang, H.-S., Chou, C.-T.: Biogas upgrading by pressure swing adsorption with design of experiments. Processes **9**, 1325 (2021)
8. Marcinek, A., Guderian, J., Bathen, D.: Process intensification of the high-purity nitrogen production in twin-bed pressure swing adsorption plants. Adsorption **27**, 937–952 (2021)
9. Xiao, J., Mei, A., Tao, W., Ma, S., Bénard, P., Chahine, R.: Hydrogen purification performance optimization of vacuum pressure swing adsorption on different activated carbons. Energies **14**, 2450 (2021)
10. Ahn, H., Hong, S.-H., Zhang, Y., Lee, C.-H.: Experimental and simulation study on CO 2 adsorption dynamics of a zeolite 13X column during blowdown and pressurization: implications of scaleup on CO2 capture vacuum swing adsorption cycle. Ind. Eng. Chem. Res. **59**, 6053–6064 (2020)
11. Marx, D., Joss, L., Hefti, M., Mazzotti, M.: Temperature swing adsorption for postcombustion CO 2 capture: single- and multicolumn experiments and simulations. Ind. Eng. Chem. Res. **55**, 1401–1412 (2016)
12. Thomass, W.J., Crittenden, B.: Adsorption Technology & Design. Elsevier Science & Technology Books, Amsterdam (1998)
13. Shirley, A.I., Lemcoff, N.O.: Air separation by carbon molecular sieves. Adsorption **8**, 147–155 (2002)
14. Gertenbach, D., Cooper, B.L.: Scale-up Issues From Bench to Pilot: Paper 509f, presented at the AIChE National Meeting, November 12, 2009. TN, Hazen Research, Inc, Nashville (2009)
15. Kast, W.: Adsorption aus der Gasphase: Ingenieurwissenschaftliche Grundlagen und Technische Verfahren. VCH Verlagsgesellschaft, Weinheim (1988)
16. Ruthven, D.M.: Principles of Adsorption & Adsorption Processes. John Wiley & Sons, Hoboken (1984)
17. Carberry, J.J.: Chemical and Catalytic Reaction Engineering. McGraw-Hill, New York (1976)
18. Koekemoer, A., Luckos, A.: Effect of material type and particle size distribution on pressure drop in packed beds of large particles: Extending the Ergun equation. Fuel **158**, 232–238 (2015)
19. Moran, A., Patel, M., Talu, O.: Axial dispersion effects with small diameter adsorbent particles. Adsorption **24**, 333–344 (2018)
20. Inglezakis, V.J., Poulopoulos, S.G.: Dispersion coefficients in fixed beds packed with irregular-shaped particles: Conference Paper, 7th World Congress of Chemical Engineering at Glasgow, Scotland (2005).
21. Sandeep, K.C., Shinde, S et al., Estimation of axial dispersion coefficient in packed beds for high pressure drop: Conference Paper, CHEMCON 2016 at Chennai (2016).
22. Kannan, P., Pal, P., Banat, F.: Design of adsorption column for reclamation of methyldiethanolamine using homogeneous surface diffusion model. Oil Gas Sci. Technol. – Rev. IFP Energies nouvelles **75**(82), 1–12 (2020)
23. Delgado, J.M.P.Q.: A critical review of dispersion in packed beds. Heat Mass Transfer **42**, 279–310 (2006)
24. LeVan, M., Vermeulen, T.: Channeling and bed-diameter effects in fixed-bed adsorber performance. AIChE Symp. Series **233**, 34–43 (1984)
25. Rastegar, S.O., Gu, T.: Empirical correlations for axial dispersion coefficient and Peclet number in fixed-bed columns. J. Chromatogr. A **1490**, 133–137 (2017)
26. Gibilaro, L.G.: Fluidization-Dynamics: The Formulation and Applications of a Predictive Theory for the Fluidized State. Butterworth-Heinemann, Oxford (2001)
27. Zhang, X., Lu, Y., Li, Y., Zhang, C., Wang, R.: Numerical calculation and experimental study on response characteristics of pneumatic solenoid valves. Meas. Control **52**, 1382–1393 (2019)
28. Stinn, M., Vance, J.: Selecting valves for pressure swing adsorption, (2018)
29. Auerbach, S.M., Carrado, K.A., Dutta, P.K.: Handbook of Zeolite Science and Technology. CRC Press, Boca Raton (2003)
30. Ruthven, D.M., Farooq, S., Knaebel, K.S.: Pressure Swing Adsorption. VCH, Weinheim (1996)
31. Marcinek, A., Guderian, J., Bathen, D.: Performance determination of high-purity N2-PSA-plants. Adsorption **26**, 1215–1226 (2020)
32. Marcinek, A.: Modelling and Simulation of Twin-Bed Pressure Swing Adsorption Plants for the Generation of High-Purity Nitrogen. Universität Duisburg-Essen, Duisburg (2021)
33. Marcinek, A., Möller, A., Guderian, J., Bathen, D.: Dynamic simulation of high-purity twin-bed N2-PSA plants. Adsorption **27**, 1149–1173 (2021)
34. Da Silva, F.A., Silva, J.A., Rodrigues, A.E.: A general package for the simulation of cyclic adsorption processes. Adsorption **5**, 229–244 (1999)
35. Rumbo Morales, J.Y., et al.: Review of the pressure swing adsorption process for the production of biofuels and medical oxygen: separation and purification technology. Adsorpt. Sci. Technol. **2022**, 1–50 (2022)
36. Sereno, C., Rodrigues, A.: Can steady-state momentum equations be used in modelling pressurization of adsorption beds? Gas Sep. Purif. **7**, 167–174 (1993)
37. Ackley, M.W.: Medical oxygen concentrators: a review of progress in air separation technology. Adsorption **25**, 1437–1474 (2019)